Measurement and Modeling of McKibben Pneumatic Artificial Muscles

Ching-Ping Chou and Blake Hannaford, *Member, IEEE*

***Abstract*—This paper reports mechanical testing and modeling results for the McKibben artificial muscle pneumatic actuator. This device, first developed in the 1950's, contains an expanding tube surrounded by braided cords. We report static and dynamic length-tension testing results and derive a linearized model of these properties for three different models. The results are briefly compared with human muscle properties to evaluate the suitability of McKibben actuators for human muscle emulation in biologically based robot arms.**

I. Introduction

THE McKibben pneumatic artificial muscle was developed in artificial limb research in the 1950's and 1960's [4], [17]. They have recently been commercialized by the Bridgestone Rubber Company of Japan for robotic applications [12], and re-engineered by Dr. J. Winters for construction of biomechanically realistic skeletal models. McKibben muscles consist of an internal bladder surrounded by a braided mesh shell (with flexible yet nonextensible threads) that is attached at either end to fittings or to some tendon-like structure (Fig. 1(a)). When the internal bladder is pressurized, the high pressure gas pushes against its inner surface and against the external shell, and tends to increase its volume. Due to the nonextensibility (or very high longitudinal stiffness) of the threads in the braided mesh shell, the actuator shortens according to its volume increase and/or produces tension if it is coupled to a mechanical load. This physical configuration causes McKibben muscles to have variable-stiffness spring-like characteristics, nonlinear passive elasticity, physical flexibility, and very light weight compare to other kinds of artificial actuators [9].

The relationships between tension, length, velocity, and activation are major characteristics of actuators which vary greatly from type to type. Human skeletal muscle also has its own particular characteristics: for example, the convex shape active tension-length relationship [5], the nonlinear passive tension-length relationship, and the hyperbolic tension-velocity relationship [11]. Each of these properties is also a function of activation level [14], [18], [19]. In order to show the similarity (or not) to biological muscles, three types of McKibben muscles, two designed and made by Dr. Winters and one manufactured by Bridgestone, were tested. Also, since the actuator is pneumatically driven, experiments and modeling on simple pneumatic circuits were included.

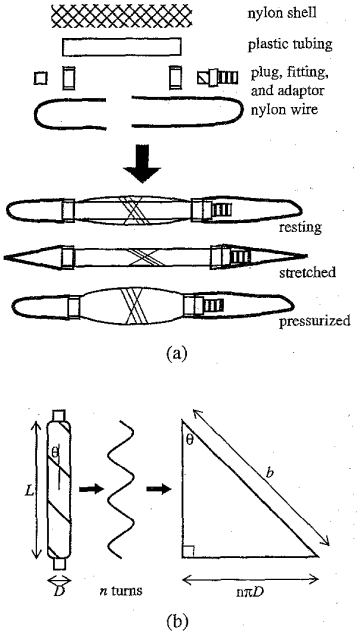

Fig. 1. Geometry of actuator. Middle portion of the actuator is modeled as perfect cylinder with length L, diameter D. θ, angle between braided thread and cylinder long axis, n, number of turns of thread, and b, thread length. Relationship between above parameters is illustrated by triangle.

In this article, all of the experiments, theories, modeling, and simulations are grouped into four major sections: Section II, quasi-static and dynamic tension-length relationships; Section III, pneumatic circuits; Section IV, isometric and isotonic experiments; and Section V, energy conversion and efficiency estimation. In Section II: 1) an idealized static physical model of McKibben muscles will be analyzed with a simple theoretical approach; 2) a dynamic testing machine will be described; 3) a series of quasi-static and dynamic experiments will be described, which show a velocity insensitive tension- length hysteresis; 4) a simplified static model will be described based on both experimental data and a theoretical approach; and 5) the quasi-static and dynamic characteristics will be analyzed. In Section III: 1) two dynamic experiments will be described with simple pneumatic circuits and 2) lumped parameter models with linear or nonlinear gas resistance will be described and simulated. In Section IV, isometric and isotonic experiments related to the pneumatic behavior will be shown. In Section V, energy conversion and

Manuscript received November 12, 1993; revised May 15, 1995. This work was supported by the Office of Naval Research under Grant N00014-92-J-1401.

The authors are with the Department of Electrical Engineering, University of Washington, Seattle, WA 98195 USA.

Publisher Item Identifier S 1042-296X(96)00488-5.

efficiency based on gas dynamics and thermodynamics will be estimated.

Finally, the actuators and pneumatic system will be compared to biological muscles. In general, the McKibben artificial muscle is much more similar to biological muscles than other kinds of artificial actuators. However, the pneumatic system, which provides control and power to the actuator, still needs a lot of improvement in order to be implemented into a feasible, independent system.

II. Static and Dynamic Tension-Length Relationships

McKibben muscle is an actuator which converts pneumatic (or hydraulic) energy into mechanical form by transferring the pressure applied on the inner surface of its bladder into the shortening tension. To find the relationship of the tension, length, and pressure, a theoretical approach and several experiments will be analyzed with simplified modeling.

A. Static Physical Model of McKibben Muscles

In order to find the tension as a function of pressure and actuator length without considering the detailed geometric structure, a theoretical approach based on energy conservation is introduced first.

The input work (W_{in}) is done in the McKibben muscle when gas pushes the inner bladder surface. This is

$$dW_{\text{in}} = \int_{S_i} (P - P_0) d\mathbf{l}_i \cdot d\mathbf{s}_\mathbf{i} = (P - P_0) \int_{S_i} d\mathbf{l}_i \cdot d\mathbf{s}_\mathbf{i} = P' dV \tag{1}$$

where P is the absolute internal gas pressure, P_0, the environment pressure (1 atm = 1.0336 bar), P', the relative pressure, S_i, the total inner surface, $d\mathbf{s}_\mathbf{i}$, the area vector, $d\mathbf{l}_\mathbf{i}$, the inner surface displacement, and dV, the volume change. The output work (W_{out}) is done when the actuator shortens associated with the volume change, which is

$$dW_{\text{out}} = -F dL \tag{2}$$

where F is the axial tension, and dL, the axial displacement. From the view of energy conservation, the input work should equal the output work if a system is lossless and without energy storage. Assume the actuator is in this ideal condition. We can then use the "virtual work" argument

$$dW_{\text{out}} = dW_{\text{in}} \tag{3}$$

thus, from (1) and (2),

$$-F dL = P' dV \tag{4a}$$

$$F = -P' \frac{dV}{dL}. \tag{4b}$$

To estimate dV/dL, first we assume the extensibility of the shell threads is very low (as it has to be chosen), so the actuator volume will only depends on its length. In addition, the middle portion of the actuator is modeled as a perfect cylinder with zero-wall-thickness (Fig. 1(b)), where L is the length of the cylinder, θ, the angle between a braided thread and the cylinder long axis, D, the diameter of the cylinder, n, number of turns of a thread, and b, the thread length. L and D can be expressed as functions of θ with constant parameters n and b,

$$L = b \cos\theta \tag{5}$$

$$D = \frac{b \sin\theta}{n\pi}. \tag{6}$$

The volume of the cylinder is

$$V = \frac{1}{4}\pi D^2 L = \frac{b^3}{4\pi n^2} \sin^2\theta \cos\theta. \tag{7}$$

So, from (4b), F can be expressed as a function of P' and θ,

$$F = -P' \frac{dV}{dL} = -P' \frac{dV/d\theta}{dL/d\theta} = \frac{P' b^2 (2\cos^2\theta - \sin^2\theta)}{4\pi n^2} = \frac{P' b^2 (3\cos^2\theta - 1)}{4\pi n^2} \tag{8a}$$

which is equivalent to

$$F = \frac{\pi D_0^2 P'}{4} (3\cos^2\theta - 1) \tag{8b}$$

where $D_0 = b/n\pi$, is the diameter when θ equals 90°, which is the same form used in Schulte's paper [17]. The tension is thus linearly proportional to the pressure, and is a monotonic function of the braid angle ($0° < \theta < 90°$). The maximal shortening will be reached when $F = 0$, that is, $\theta = 54.7°$.

Notice that although we obtained the tension with the assumption of ideal cylinder here, the tension can always be derived by knowing the dV/dL of any arbitrary shape actuator with (4b) without the assumption.

The physical nonideality of the actuator will be considered while analyzing the experimental results later.

B. Dynamic Testing Machine

For the following experiments, a testing system capable of producing and recording desired patterns of the tension, length, and pressure of the actuator was built (Fig. 2). The system consists of an IBM compatible personal computer (PC, with 16 MHz 386sx, real time updating rate up to 5 kHz), PC extension bus interface and timer circuit, A/D, D/A converters, analog filters and amplifiers, pressure sensors (6.8 bar max.), strain gauge force sensors (100 N max.), filters, amplifiers, a 1/4 horse power dc motor with PWM power amplifier (±24 A max. current), an optical angular position incremental encoder (1600 steps per revolution) and a decoder, a pressure regulator (10 bar max.), an electrovalve (Festo proportional pressure regulator MPP-3-1/8, 10 bar max.), two gas accumulators (3 in^3 and 10 in^3), and flexible tubing ($\phi 1/8''$).

By utilizing different combinations of the I/O channels and software settings, the system can performs a variety of testing conditions, such as constant pressure testing, isometric testing, isotonic testing, pneumatic circuit testing, etc.

C. Quasi-Static and Dynamic Experiments

Since there is no analytical solution to describe biological muscle tension-length-activation relationship, a variety of testing configurations have been chosen to illustrate part of this relationship, such as static tension-length relation under

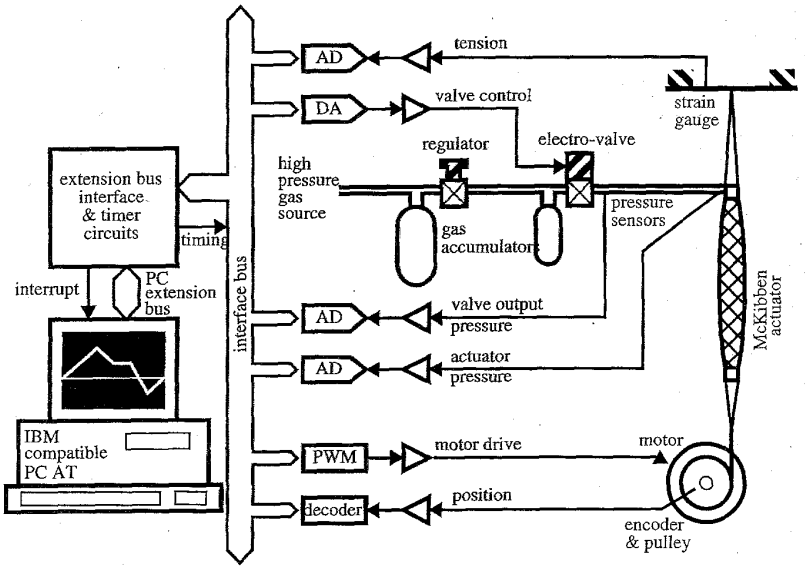

Fig. 2. Block diagram of dynamic testing machine.

constant activation level [5], isometric to isotonic quick release experiment [3], isokinetic experiment [3], [13], isometric tension in response to activation [1], [2], etc. Notice that the activation is always an input to muscle mechanics, and either one of the other two quantities (tension and length) may be input or output. The pressure of the actuator is analogous to the activation level and will initially be thought of as an input to the actuator, which will be held as constant as possible in these experiments in order to minimize the effects of the pressure dynamics and thus simplify the analysis.

Three types of actuators were tested in quasi-static experiments and one was also tested in dynamic experiments. The first one, with nylon shell, is 14 cm resting length, and 1.1 cm in diameter at 5 bar no load. The second one, with fiberglass shell, is 20 cm in length, 0.9 cm in diameter. And the third one, manufactured by Bridgestone, is 14.7 cm in length, 1.5 cm in diameter.

In quasi-static experiments, first, the nylon shell actuator was tested. A set of low frequency triangular wave displacements (relative to resting length, $L_0 = 14$ cm) to best cover the linear tension regions corresponding to different pressure levels are selected as the input. The displacements are set to 1 Hz with large operating range (which yields the peak velocity about 0.5 L_0/s).

The pressure is set by a manual regulator to obtain six desired constant levels (0–5 bar relative). Due to: 1) the volume change of the actuator with length change; 2) the gas viscosity in connection tubing; and 3) the regulator's output hysteresis, the measured pressure will increase when the actuator lengthens and will decrease when it shortens. In order to reduce the variation of the pressure, a 10 in^3 (164 cm^3) accumulator is connected to the regulator, and a 3 in^3 (49 cm^3) accumulator is connected directly to the actuator. As a result, the pressure variation was limited to less than 0.1 bar due to the large total capacity of the accumulators, and the pressure hysteresis is almost immeasurable due to the close position (to the actuator) of the second accumulator.

Both the measured pressure and the tension are shown in response to the displacements (Fig. 3(a)). By minimizing the effect of pressure variation, the hysteresis loop of the tension-length relationship is illustrated. The width and height of the loop is about 0.2–0.5 cm and 5–10 N, respectively. Two further experiments were made to illustrate more features of the hysteresis.

First, the frequency of the displacement waveforms is reduced to 0.25 Hz, while the operating range remains the same (which yields the peak velocity about 0.125 L_0/s). The result is almost identical to the previous case, which suggests that the tension-length behavior is velocity independent at low velocities. Second, the frequency is set to 1 Hz, while the operating range is reduced about half (Fig. 3(b), solid lines). The tension rising paths remain the same (the rising "initial conditions" are the same), but the falling paths are different (The falling "initial conditions" are different due to the smaller operating range). Thus the width and height of the loop are reduced. This indicates the hysteresis is history dependent.

The procedures to obtain Fig. 3(a) were repeated for the other two actuators, and the results in the same format are shown in Fig. 3(c) and (d). The stiffness, friction, and extensibility are quite different in the above three actuators.

In dynamic experiments, a set of middle to high frequency sinusoidal displacement waveforms (relative to zero tension length) with small operating range are applied to the first actuator. The pressure is set to relative 5 bar, and remains constant quite well in this condition (due to smaller length change). The frequencies and displacement ranges are designed to obtain 0.2–8.0 L_0/s peak velocity yet remain in the linear tension-length region. The viscous friction (damping force) if measurable, would be revealed by a hysteresis width which is

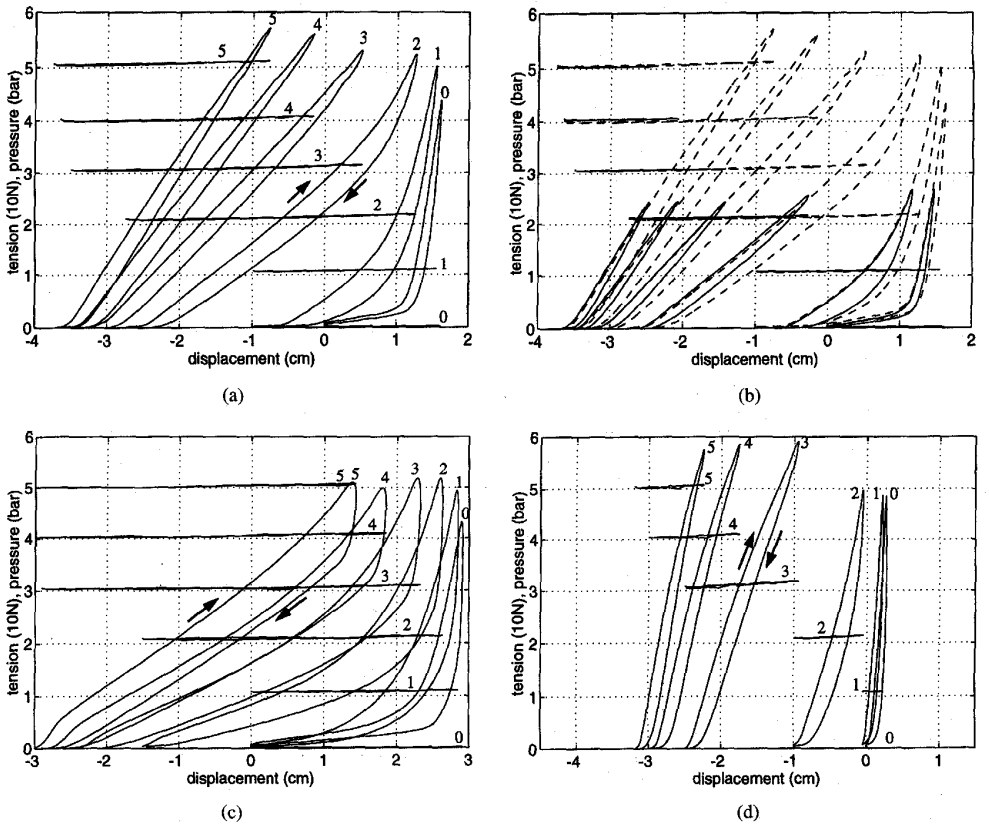

Fig. 3. Quasi-static experiments. (a) and (b) are X-Y plots of experimental results for nylon shell actuator. Six pairs of curves are superimposed in plots: nearly horizontal curves, measured pressure-length, sloped curves, tension-length. Operating pressure in bar is printed just above each tension-length loop. Hysteresis direction is clockwise. (a) Large range, 1 Hz. (b) Small range, 1 Hz. (c) X-Y plot of experimental results for fiberglass shell actuator. (d) X-Y plot of experimental results for Bridgestone actuator.

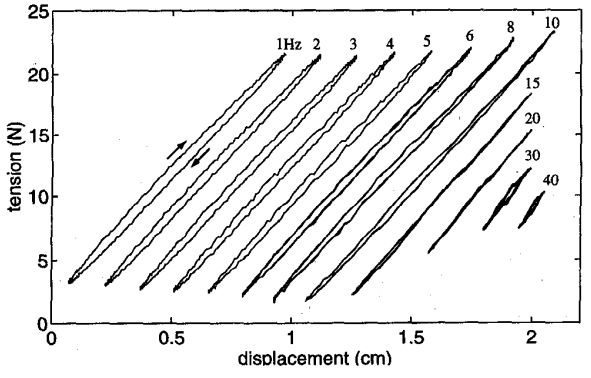

Fig. 4. X-Y plot of dynamic sinusoidal responses. Results for 12 frequencies are combined together with shifting curves along displacement axis. Notice width of hysteresis is almost unchanged for peak velocity from 0.2 L_0/s (1 Hz) to 2.0 L_0/s (10 Hz). Hysteresis direction is clockwise.

a monotonic increasing function of the velocity. However, the results show that the width of the tension-displacement loop is almost unchanged, except for a slight decrease at higher frequency (Fig. 4).

These results indicate that the velocity-independent hysteresis is most likely to be the Coulomb friction, which dominates the total friction of the actuator. The viscous friction is much smaller than Coulomb friction and thus immeasurable.

D. Simplified Static Model

Excluding the above Coulomb friction, a hypothetical static tension-length relation can be calculated including a correction for the wall thickness if desired. From (8b), the tension is linearly proportional to the pressure, and is a monotonic function of the braid angle ($0° < \theta < 90°$). By applying the geometry parameters (measured from the nylon shell actuator, $b = 16.4$ cm, $n = 3.15$, and yields $D_0 = 1.66$ cm) to (8b), the simulation result is shown in Fig. 5(a)–(d) (solid lines). However, if the thickness (t_k) of the shell and bladder is considered, the relation becomes

$$V = \frac{1}{4}\pi(D - 2t_k)^2 L \tag{9}$$

by plugging into (4b),

$$F = -P'\frac{dV}{dL} = \frac{\pi D_0^2 P'}{4}(3\cos^2\theta - 1) + \pi P'\left[D_0 t_k\left(2\sin\theta - \frac{1}{\sin\theta}\right) - t_k^2\right]. \tag{10}$$

This is more accurate but more complex than (8b) (Fig. 5(a)–(d) dashed line, with $t_k = 0.0762$ cm in addition).

In order to simplify the model, the tension is now considered as a function of the pressure and the length, and the actuator is just like a variable-stiffness elastic element, or a "gas spring."

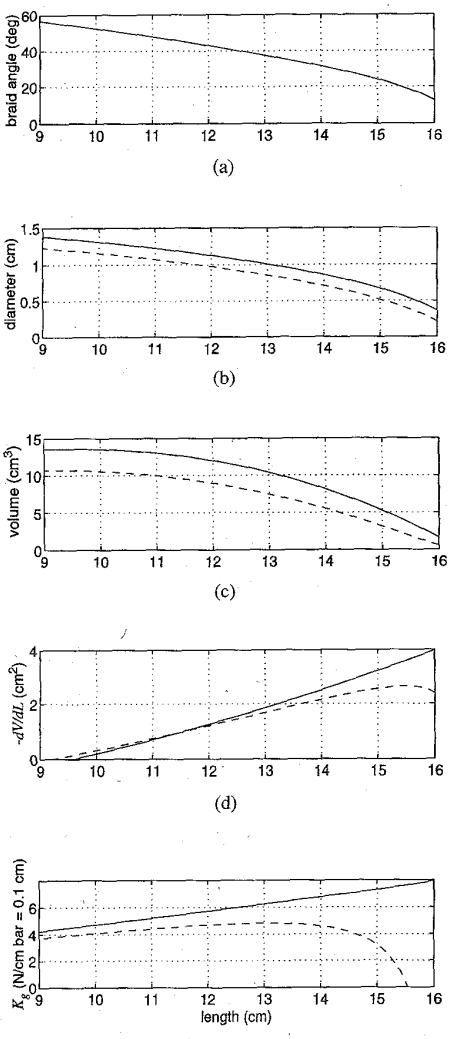

Fig. 5. (a)–(e) Simulation results of nylon shell actuator's static characteristics as function of length. Dashed lines, results considering thickness of braided shell and bladder, solid lines, results without considering wall thickness.

Its stiffness ($K \equiv dF/dL$) is proportional to the pressure, and the stiffness per unit pressure ($K_g \equiv dK/dP'$) approximates a constant within 10 to 14 cm length by simulation (Fig. 5(e), $K_g = 0.461$ cm, or 4.61 N/cm · bar). As a result, it can be linearized as

$$F = K_g P'(L - L_{\min}) \tag{11}$$

where $L_{\min}$ is the theoretically possible minimum length (when $F = 0$).

Now, considering energy stored by the actuator in its bladder and shell, yields

$$F = K_g(P' - P_{\text{th}})(L - L_{\min}) + K_p(L - L_0) + \text{nl}(L) \quad \text{if } P' > P_{\text{th}} \text{ or} \tag{12a}$$

$$F = K_p(L - L_0) + \text{nl}(L) \quad \text{if } P' \le P_{\text{th}} \tag{12b}$$

where P_{th} is the threshold for the pressure to overcome the radial elasticity of the bladder for expanding, K_p is the linearized equivalent parallel passive elastic constant for the shearing force of the bladder material and shell threads, and $\text{nl}(\cdot)$ is the nonlinear term due to the nonperfect cylinder while the actuator is at its extreme length (Fig. 6(a)). The first two product terms in (12a) can also be expressed as

$$F = K_g(P' - P_a)(L - L_{\min}) + F_a \tag{13}$$

where $P_a = P_{\text{th}} - K_p/K_g$, and $F_a = K_p(L_{\min} - L_0)$. To experimentally estimate these parameters, 10 points of hypothetical static tension-length-pressure pairs are sampled from above quasi-static results and fit into (13) (Fig. 6(b)). This calculation gives $K_g = 0.466$ cm, $P_a = 0.062$ bar, $L_{\min} = 9.91$ cm, and $F_a = -16.0$ N. Also, P_{th} and K_p can be estimated by knowing $L_0 = 14.0$ cm, which yields $P_{\text{th}} = 0.903$ bar and $K_p = 3.92$ N/cm. Notice the K_g is very close to the simulation value (0.461 cm) of the theoretical model. The nonlinear term only becomes significant when the actuator is extremely short or extremely long, usually this is out of regular operating range, and will not be discussed further.

E. Quasi-Static and Dynamic Characteristics

It has been shown that there is hysteresis in the tension-length cycle, and that the dominant friction is the frequency insensitive Coulomb friction, which is caused by the contact between the bladder and the shell, between the braided threads and each other, and the shape changing of the bladder. The history dependence makes the friction difficult to predict precisely, especially after the actuator is attached to artificial bones with curving shape. So, it is suggested to add a typical friction value (±2.5 N, positive for lengthening, negative for shortening) to the hypothetical static equation ((12a) or (13) and (12b)) if a simple friction model is sufficient.

III. Pneumatic Circuits

Since the McKibben actuator is driven by pneumatic power, it is important to understand some basic phenomena of the pneumatic dynamics in order to distinguish the factors of pneumatic circuit from those of the actuator mechanics.

A. Pressure Dynamic Experiments in Pneumatic Circuits

The most important state variables in a pneumatic circuit are pressure and mass flow. The pressure can be measured directly, and the mass flow can be derived from the changing of the pressure in an accumulator.

Two pressure dynamic experiments were made with simple pneumatic circuits as shown in Fig. 7(a) including an electrovalve, which produces a nonperiodical pressure waveform, pneumatic tubing (ϕ 1/8″, length 100 cm), which introduces gas viscosity, an accumulator, which behaves as a capacitor, and two pressure sensors, one at the connection of the electrovalve output and the tubing (P_1), and the other at the connection of the tubing and the accumulator (P_2). The configurations of the two experiments are similar except the volume of one accumulator is 164 cm^3 (10 in^3) and the other is 49 cm^3 (3 in^3). The experimental results of the pressure

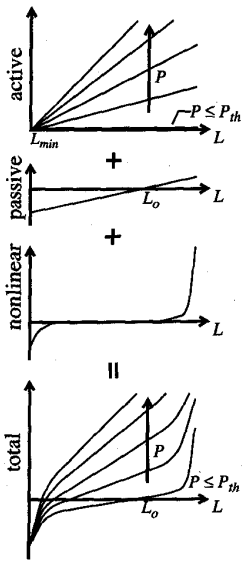

(a)

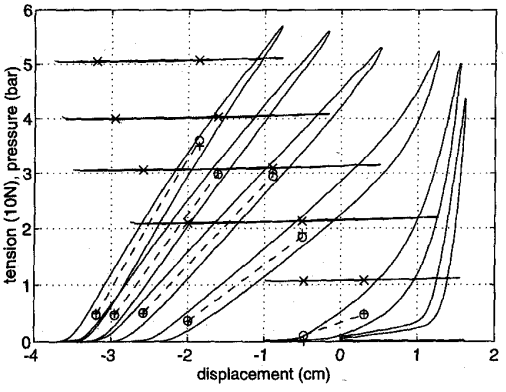

(b)

Fig. 6. Static model of actuator. (a) Total tension is summation of active term, passive term, and nonlinear term. (b) Parameters of linearized model are optimized with 10 tension-length-pressure sample points from experimental data of Fig. 3(a). x, sampled pressure, +, sampled tension, o, simulation tension.

responses will be shown with simulation results later. The modeling is limited to the response of P_2 to P_1, which includes the pneumatic characteristics of the tubing and the accumulator. However, the modeling of the electrovalve is not covered, because it is too complex to obtain an accurate yet simple model.

B. Lumped-Parameter Models of Pneumatic Circuits

To analyze a pneumatic circuit (even as simple as the above ones) is not easy in fluid dynamics. There are at least three reasons to explain that. First, it is a distributed-parameter system. The state variables are not only functions of time, but also functions of space; alternatively, there are infinite number of discrete state variables theoretically. Second, it is very sensitive to geometry. All of the time-varying boundary conditions must be met to solve the gas momentum equation

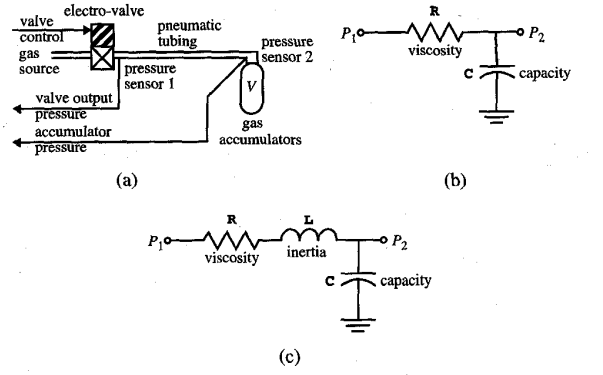

(a) (b) (c)

Fig. 7. (a) Pneumatic circuit configuration. (b) Circuit notation of lumped parameter model with capacity and viscosity. (c) Circuit notation of lumped parameter model with additional inertia.

[15],

$$\frac{D\mathrm{v}}{Dt} = -\frac{1}{\rho}\nabla P + \nu\nabla^2\mathrm{v} + \frac{1}{3}\nu\nabla(\nabla\cdot\mathrm{v}) + \sum \mathrm{F} \qquad (14)$$

and the energy equation,

$$\frac{\rho D(u+\mathrm{v}^2/2)}{Dt} = \nabla\cdot P\mathrm{v} + \rho\sum \mathrm{F}\cdot\mathrm{v} + \nabla\cdot k\nabla T + \sum Q \qquad (15)$$

where $D/Dt \equiv \partial/\partial t + \mathrm{v}\cdot\nabla$, ∇, gradient operator, $(\nabla\cdot)$, divergence operator, (∇^2), Laplacian operator, v, gas velocity, ρ, density, P, pressure, ν, kinematic viscosity, F, any body force, u, internal energy, k, thermal conductivity, T, temperature, and Q, any other energy-transfer mechanism. Third, as the flow velocity rises, turbulent flow gradually takes over laminar flow. After that, it is impossible to obtain an analytical solution, and the system can only be solved by some powerful simulation program for a period of time.

The computation time will be of greater concern as the number of the actuators (and the pneumatic circuits) is increased in an application system. Lumped-parameter models with few parameters and few state variables can best meet this requirement. In the following, three models are described in the order of complexity as well as accuracy.

In the first model, two node pressures (P_1 and P_2, absolute) are the only state variables (as "effort" or voltage). The mass flow (w) through each node (as "flow" or current) can be derived from these states with the parameters. The gas viscosity caused by the tubing (and the connections) is modeled as a linear resistor (R), and the accumulator as a linear capacitor (C) (Fig. 7(b)). By ignoring the volume of the tubing, there are the relations

$$\frac{P_1 - P_2}{\mathrm{R}} = w \qquad (16)$$

$$w = -\mathrm{C}\frac{dP_2}{dt} \qquad (17)$$

which yield

$$P_1 - P_2 = \mathrm{RC}\frac{dP_2}{dt}. \qquad (18)$$

This is a linear low-pass-filter response with only one parameter ($\omega_c = 1/\mathrm{RC}$, the cut-off frequency). A simulation of this model with ω_c optimized to 4.0π yields rms error = 0.19 bar.

In the second model, the resistance is modeled as

$$P_1 - P_2 = \mathrm{R}_1\left(\frac{w}{\rho_t A_t}\right) + \mathrm{R}_2\left(\frac{w}{\rho_t A_t}\right)2 \tag{19}$$

where A_t is effective cross-section area of the tubing and connectors, R_1 and R_2 are constant and will be determined experimentally, and ρ_t is gas density inside the tubing,

$$\rho_t = \frac{P_t}{RT} \approx \frac{(P_1 + P_2)/2}{RT} \tag{20}$$

where R is gas constant per unit mass, T, temperature, and P_t is the average absolute pressure inside the tubing and is approximated to $(P_1 + P_2)/2$.

The capacitance, C, is the same as in (17), and $w \equiv dm/dt$, yields

$$\mathrm{C} = \frac{dm/dt}{dP_2/dt} = \frac{dm}{dP_2} \tag{21}$$

where m is gas mass in the accumulator. These experiments are a kind of gas "free expansion" from high pressure source into constant volume container, which is an isothermal process. Thus, C can be derived from the volume of the accumulator (V) and ideal gas equation,

$$PV = mRT \tag{22}$$

by substituting P_2 for P and using (21),

$$\mathrm{C} = \frac{V}{RT}. \tag{23}$$

By utilizing (17), (19), and (20), the accuracy of the simulation results are greatly improved (Fig. 8(a) and (b)), and R_1 and R_2 are optimized for each experiment with different V. It should be noticed that the values of R_1 and R_2 for two experiments are quite different after optimization. Also, the simulation response leads the measured response by approximately 4 ms.

The third model extends the second one by including the gas inertia (L, Fig. 7(c)),

$$\Delta P_L = \mathrm{L}\frac{dw}{dt} \tag{24}$$

where ΔP_L is the pressure difference caused by inertial load. Converting Newton's first law, $F = d(m\mathrm{v})/dt$, into pneumatic form yields

$$A_t \Delta P_L = \frac{d(\rho_t A_t l_t \mathrm{v})}{dt} \tag{25}$$

where l_t is effective length of the tubing and connectors, and v is gas velocity. Also, substitutes $w = \rho_t A_t \mathrm{v}$ into (25), giving

$$A_t \Delta P_L = \frac{dw}{dt} l_t \tag{26}$$

with (24), we obtain

$$\mathrm{L} = \frac{l_t}{A_t}. \tag{27}$$

Equation (19) now should be modified into

$$P_1 - P_2 = \mathrm{R}_1\left(\frac{w}{\rho_t A_t}\right) + \mathrm{R}_2\left(\frac{w}{\rho_t A_t}\right)^2 + \mathrm{L}\frac{dw}{dt}. \tag{28}$$

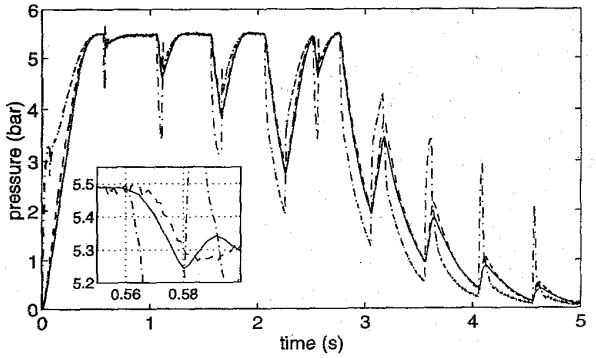

(a)

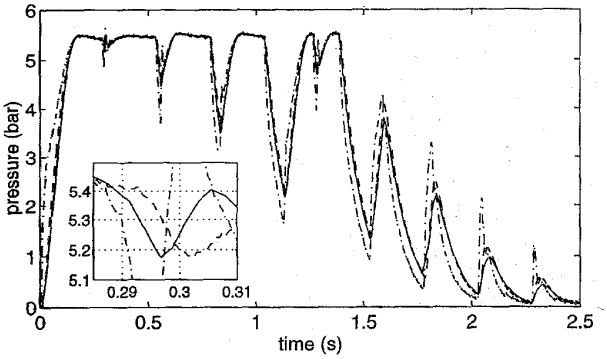

(b)

Fig. 8. Dynamic responses of pneumatic circuit with simulation results of nonlinear viscosity model. Center lines, input pressure P_1, dashed lines, measured output P_2, solid lines, simulation output P_2. (a) With accumulator $V = 10$ in^3, C = 0.190 g/bar, R_1 = 4.91e-6 bar.s/cm, R_2 = 2.07e-8 bar·s^2/cm^2, rms error = 0.111 bar. (b) With accumulator $V = 3$ in^3, C = 0.057 g/bar, R_1 = 4.50e-6 bar·s/cm, R_2 = 2.61e-8 bar·s^2/cm^2, rms error = 0.132 bar.

By utilizing (17), (20), and (28), the simulation results are shown in Fig. 9(a) and (b). R_1 and R_2 now are optimized for the experiment with 10 in^3 accumulator, and without changing those values, applied to the 3 in^3 accumulator. For both accumulators we obtain very good accuracy and a slight improvement on the second model in terms of rms error. Since the second model could only be fit to the two accumulators by re-optimizing R_1 and R_2, this model shows a significant improvement. Also, the 4 ms lead in the simulation responses of the second model disappears. This illustrates that the robustness and accuracy of the model are improved by adding a simple inertia term.

IV. Isometric and Isotonic Experiments

In these two series of experiments, some characteristics related to both the actuator and gas dynamics will be demonstrated. These will give valuable information about the timing of the response waveform and the power capability of the system. For both series, particular patterns of control voltage are input to the electrovalve to generate dynamic pressure waveforms.

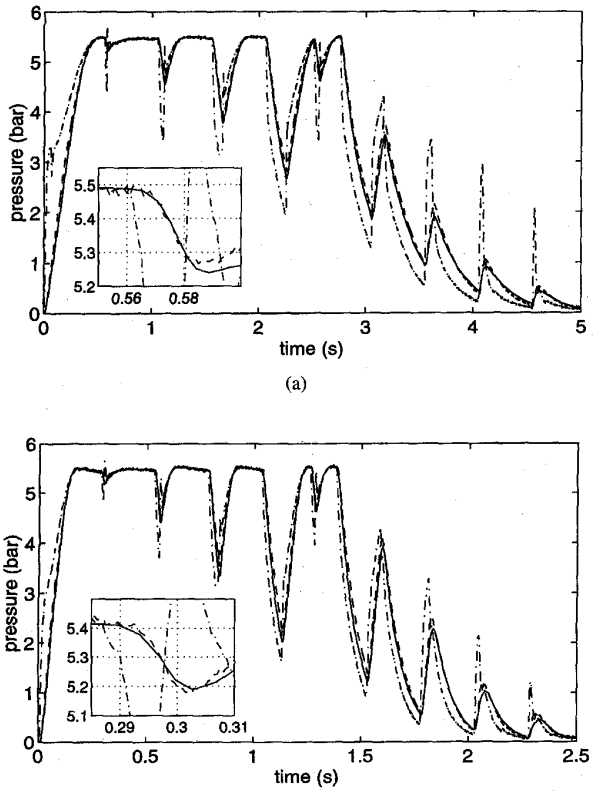

Fig. 9. Dynamic responses of pneumatic circuit with simulation results of additional inertia model. Center lines, input pressure P_1, dashed lines, measured output P_2, solid lines, simulation output P_2. L = 1.26e-3 bar·s^2/g (= 126 cm^{-1}), R$_1$ = 4.91e-6 bar·s/cm, R$_2$ = 2.07e-8 bar.s^2/cm^2. (a) With accumulator V = 10 in^3, C = 0.190 g/bar, rms error = 0.107 bar. (b) With accumulator V = 3 in^3, C = 0.057 g/bar, rms error = 0.127 bar.

A. Isometric Experiments

In these experiments, without using the motor, the actuator is fixed at the end to a stiff metal plate. The tension is recorded in response to a square wave (steps) control voltage, and the pressure recording is also shown for reference (Fig. 10). The delay time from the control voltage stepping to the pressure rising is about 5 ms, purely due to the delay of the valve. From the rise of pressure to the rise of tension is about 7 ms, mostly because it takes time for the pressure to overcome the threshold (P_{th}). The tension rising time (0 to 90%) is 30 ms for the full range step and 15 ms for the half range step, and the falling time (100% to 10%) is 53 ms and 30 ms, respectively, these are limited by the maximum flow rate of the valve and the gas viscosity of the tubing (and connectors).

B. Isotonic Experiments

In these experiments, closed loop control of the tension is performed by feeding back the measured tension to the motor drive. Three different frequency (1, 2, and 5 cycles/s) triangular waveforms are applied to the valve control voltage, and three different constant load levels are selected for the controlled tension. The pressure, shortening (negative displacement), and measured tension of selected typical results

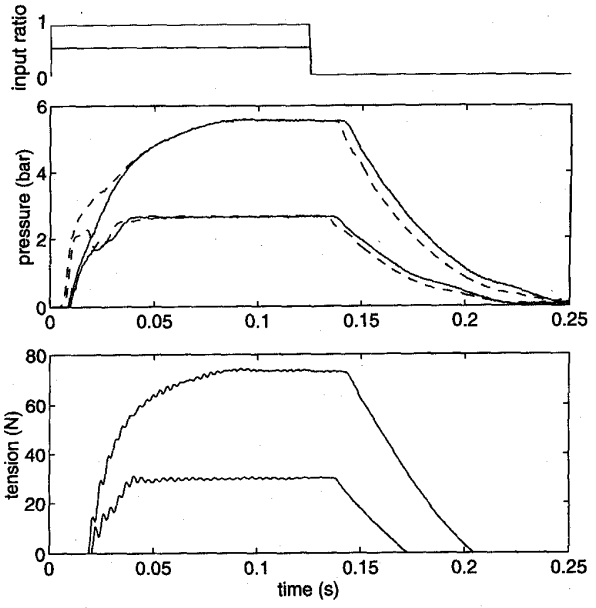

Fig. 10. Isometric step response experiments. Two sets of curves in response to two different amplitudes of control voltage steps are superimposed in plot. Upper lines, control voltage ratio, dashed lines, valve output pressure, middle solid lines, actuator pressure, lower lines, tension.

are shown in Fig. 11. The highest average velocity, 41.0 cm/s, and peak velocity, 86.6 cm/s, in these experiments are obtained at 5 cps and 10 N load. It is evident that the measured tension has some variation due to limited capability of the motor subsystem and the bandwidth of the feedback. However, the positive work and power can still be calculated by numerically integrating the product of tension and positive shortening velocity. This gave the work per each shortening of 0.45 J, average power of 0.9 W, and peak power of 3.8 W at 10 N load-1 cycle/s, or the work per each shortening of 1.4 J, average power of 14 W, and peak power of 33 W at 50 N load-5 cycle/s. These values are for reference but do not represent the maximum capability of the actuator. The maximum power is mostly limited by the maximum pressure of the gas source, the maximum flow rate of the valve, and the gas viscosity inside the pneumatic circuit.

V. Energy Conversion and Efficiency

Energy efficiency is an important factor of an actuator. In order to estimate the energy efficiency of the actuator, several specific simulations will be introduced. This will also illustrate under what condition the higher efficiency may be obtained.

According to thermodynamics, mechanical energy is transformed into gas internal energy or heat when gas is compressed, and gas internal energy or heat is transformed back to mechanical energy when gas is expanded (except free expansion). In the following, a quantitative analysis of energy conversion in a pneumatic system with the nylon shell McKibben actuator will be classified into 3 different conditions: 1) quasi-stationary, constant pressure maximal shortening; 2) quasi-stationary, isotonic shortening; and 3) constant pressure isotonic shortening. For each condition, the process of energy

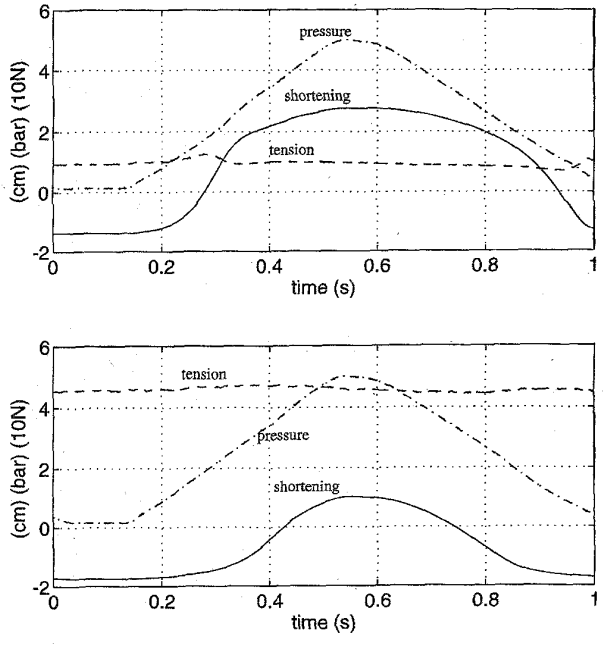

Fig. 11. Isotonic triangular response experiments. Two typical results are shown at 1 cycle/s with 10 N (top) and 50 N load (bottom), respectively. Center lines, actuator pressure, dashed lines, tension, solid lines, shortening. Power is product of tension and shortening velocity.

conversion will also be separated into several steps in each cycle.

In general, the actuator can produce positive net mechanical work if it shortens at higher pressure under larger tension and lengthens at lower pressure under smaller tension (if the tension in shortening and in lengthening is the same, there will be no net work produced). This cycle can be expressed as five steps: 1) prepare the high pressure gas source; 2) shorten under high tension; 3) exhale; 4) lengthen under low tension; and 5) inhale for the next cycle. These steps will be specified for each condition as following:

A. Quasi-Stationary, Constant Pressure Maximal Shortening Condition

In this condition, the whole cycle, except exhaling, is assumed to be processed quasi-stationarily. This will eliminate any unnecessary energy loss, and will also make the isothermal assumption very reasonable. In addition, a hypothetical compressor with piston and inhale/exhale valves will be invoked to calculate the energy for preparing the high pressure gas source, which is assumed to connect with the actuator through a zero-volume tubing.

At the beginning of each cycle, the actuator is initially stretched at zero relative pressure by a tension against the passive elasticity of the actuator, and there is a certain amount of gas inside the compressor at environment pressure (point A in Fig. 12(a) and (b)).

The volume (V, variable) in Fig. 12(a) represents the total volume of gas inside the compressor plus the initial volume of the actuator (V_2, constant, at initial length L_2, constant). And the absolute pressure (P, variable) represents the gas pressure

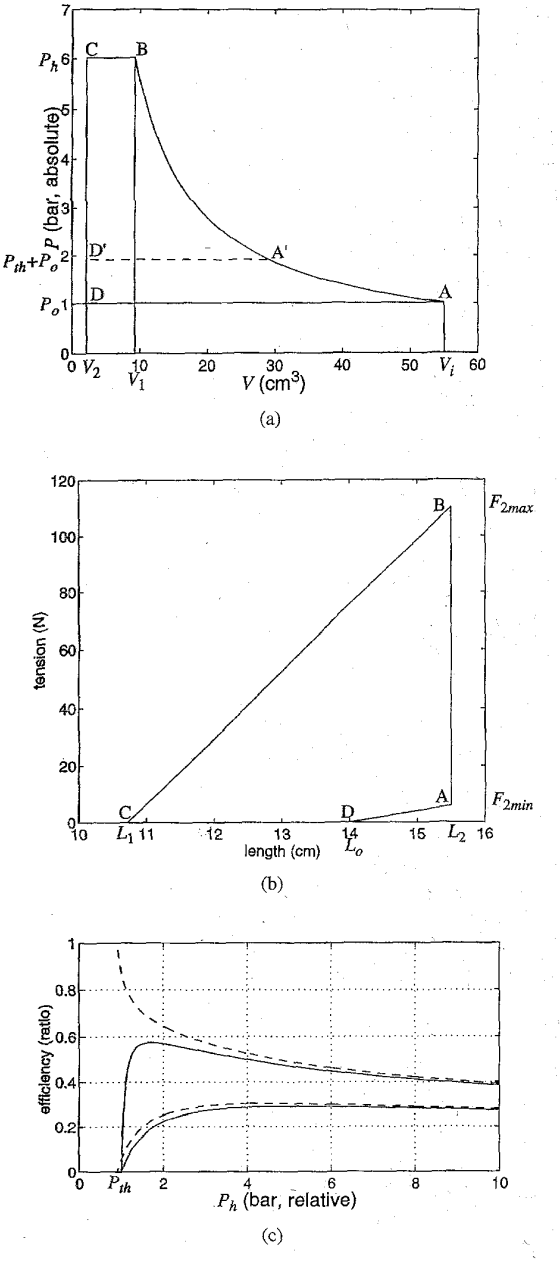

Fig. 12. Illustration of actuator's energy efficiency for quasi-stationary constant pressure shortening condition. (a) Pneumatic cycle of hypothetical compressor at $P_h = 5$ bar relative. Total input work is 8.86 J for ABCD cycle, and 5.50 J for A'BCD' cycle. (b) Mechanical cycle of actuator. Output work is 2.59 J (with 2.5 N Coulomb friction), which yields efficiencies are 0.29 and 0.49, respectively. (c) Energy efficiencies (E_a) as functions of high pressure level P_h. Lower traces, gas is exchanged from environment (ABCD cycle). Upper traces, gas is exchanged from an accumulator with absolute pressure $P_{th} + P_0$ (A'BCD' cycle). Solid lines, with 2.5 N Coulomb friction at shortening, dashed lines, without friction.

inside the compressor and the actuator. On the other hand, the length (L, variable) in Fig. 12(b) represents the length of the actuator bladder, and the tension (F, variable) represents the actuator tension at specific length and pressure.

In step 1, the pressure is increased by compressing the gas inside the compressor, while keeping the actuator isometric

by increasing the tension accordingly (A to B). In step 2, let the actuator shorten as much as possible at constant pressure (until the tension becomes zero; B to C). In step 3, exhale the gas into environment (C to D). In step 4, re-stretch the actuator to its initial length (D to A in Fig. 12(b)). Finally, in step 5, inhale the certain amount of gas from environment into the compressor (D to A in Fig. 12(a)), and return to the initial condition.

In order to analyze this cycle, there are several constants must be introduced: V_i, total initial gas volume; V_1, the maximally shortened actuator volume; P_0, the environment pressure; P_h, the high pressure while shortening; L_0, the actuator resting length; L_1, the maximally shortened length; L_2, the initial stretched length; $F_{2\min}$, the passive elastic tension at length L_2 and pressure P_0; and $F_{2\max}$, the tension at length L_2, pressure P_h, and friction $F_{\rm cf}$.

The mechanical energy applied by the piston to the gas in step 1 is

$$W_{01} = -\int_{V_i}^{V_1} (P - P_0)dV = -\int_{V_i}^{V_1} PdV - P_0(V_i - V_1) \tag{29}$$

by utilizing the ideal gas equation (see (22)), for constant mRT, yields $PV = P_0V_i = P_hV_1$, and

$$\begin{aligned} W_{01} &= -P_hV_1\int_{V_2}^{V_1}\frac{dV}{V} - P_0V_i\left(1 - \frac{P_0}{P_h}\right) \\ &= P_hV_1\left(\log\frac{P_h}{P_0} - 1 + \frac{P_0}{P_h}\right). \end{aligned} \tag{30}$$

In addition, the maximally shortened length L_1 and V_1 are determined only by P_h. So W_{01} can be represented as a function of P_h only. To estimate L_1, the linearized tension-length-pressure equation as described in (13) is solved by assigning $F = F_{\rm cf}$ ($F_{\rm cf}$ is the estimated Coulomb friction), $P' = P_h - P_0$, and $L = L_1$, thus

$$L_1 = L_{\min} + \frac{F_{\rm cf} - F_a}{K_g(P_h - P_0 - P_a)}. \tag{31}$$

And to estimate V_1 based on the same linearized model, (4b is applied reversely with considering the offsets (pressure threshold and passive elasticity), which becomes

$$V = -\frac{K_g}{2}(L - L_0)^2 - K_g(L_0 - L_{\min})(L - L_0) + V_0. \tag{32}$$

And V_1 is obtained by substituting L_1 for L.

The work input by the piston in step 2 is

$$W_{12} = (P_h - P_0)(V_1 - V_2) \tag{33}$$

which is also a function of P_h only.

The net work output by the actuator is equivalent to the area of tetragon ABCD in Fig. 12(b),

$$W_a = \frac{1}{2}[(L_2 - L_1)F_{2\max} - (L_2 - L_0)F_{2\min}] \tag{34}$$

which is a function of L_1, therefore, is a function of P_h only.

Now, the efficiency of energy conversion can be calculated as

$$E_a = \frac{W_a}{W_{01} + W_{12}} \tag{35}$$

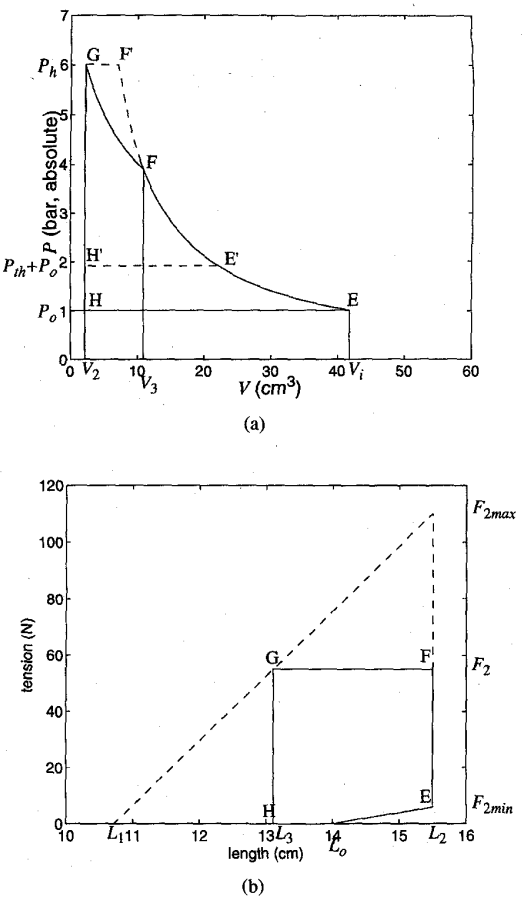

Fig. 13. Illustration of actuator's energy efficiency for quasi-stationary isotonic shortening and constant pressure isotonic shortening conditions. (a) Pneumatic cycle of hypothetical compressor at $P_h = 5$ bar relative. Total input works are 5.79 J for EFGH cycle, 3.29 J for E'FGH' cycle, 6.46 J for EF'GH cycle, and 3.96 J for E'F'GH' cycle. (b) Mechanical cycle of actuator. Output work is 1.27 J (with 2.5 N Coulomb friction), which yields efficiencies are 0.22, 0.39, 0.20, and 0.32, respectively.

which shows the maximum efficiency is about 0.3 at $P_h = 5$ bar relative pressure, decreases slowly for higher pressure, and decreases to zero very fast for lower pressure when the pressure approaches the threshold $P_{\rm th}$ (Fig. 12(c)). Notice that W_a is always less than W_{12}, and W_{01} is wasted totally when exhaling (free expansion).

B. Quasi-Stationary, Isotonic Shortening Condition

In this condition, the whole cycle, except exhaling, is assumed to be processed quasi-stationarily. The initial condition (point E in Fig. 13(a) and (b)) and step 1 (E to F) are the same as in the previous case (except different values). In step 2, let the actuator shorten isotonically while continuing to increase the pressure (F to G). Step 3 (G to H), step 4 (H to E in Fig. 13(b)), and step 5 (H to E in Fig. 13(a)) are again the same as in the previous case.

The variables and constants in Fig. 13(a) and (b) have the same meaning as in Fig. 12(a) and (b). In addition, the constant V_3 indicates the volume of the actuator at length L_3, and F_2 is the isotonic tension which is chosen to $(F_{2\max} + F_{2\min})/2$.

Due to the complexity of analytical approach for this isotonic case, only one value of the efficiency is calculated numerically by integrating those two loops with P_h at 5 bar relative pressure. This obtains $E_b = 0.22$.

C. Constant Pressure Isotonic Shortening Condition

In step 2 of the second case, the pressure is increased according to the isotonic requirement while the actuator is shortening, however, the compressor may not be so "programmable" to produce the pressure pattern, or, this "hypothetical" compressor may be replaced by a valve and supply in actual implementations. So, instead of moving from point E through F to G in the second case, the P-V states go from point E through F′ to reach P_h while compressing, then go to G with constant pressure (Fig. 13(a)). The additional energy (area FF′G) is wasted by the pressure-reducing mechanism of the valve and the gas viscosity in the pneumatic circuit under nonstationary condition. This yields the efficiency, $E_c = 0.20$.

D. Efficiencies Improvement

A feasible way to improve the efficiency is to inhale/exhale gas from/to an accumulator with internal pressure equal to the threshold ($P_{\text{th}} + P_0$ absolute) instead of from/to environment (P_0 absolute). This will not effect the output work done by the actuator, but will reduce the input work done by the piston, which is equivalent to reducing the area from ABCD of Fig. 12(a) to A′BCD′, and from EFGH of Fig. 13(a) to E′FGH′, respectively. For the case $P_h = 5$ bar relative, the new value of E_a is 0.49, E_b is 0.39, and E_c is 0.32. This is much higher than before.

VI. Discussion

In the following, comparisons will be given between the McKibben muscles and biological skeletal muscles in terms of static properties, dynamic properties, and energy efficiencies. Selected properties of the supplementary pneumatic elements will also be evaluated.

A. Static Properties: Tension-Length-Activation Relationships and Output Work

The general shape of the tension-length curve of the actuators is a monotonic increasing function of the length. For the tested nylon shell actuator, the tension reaches zero when the length is shorter than 0.75 L_0 ($L_0 = 14$ cm), and becomes very stiff when the length is longer than 1.1 L_0. Between these two points, the stiffness is about constant with a typical value of 22.4 N/cm (314 N/L_0) at 5 bar, and is approximately proportional to the pressure with some offset. The maximum tension is 110 N at 1.1 L_0 and 5 bar. The integration of the tension within 0.75 to 1.1 L_0 is 19 NL_0, which is the maximum output work per each mechanical cycle.

In order to calculate the stiffness and tension intensities per unit cross section area and the work per unit volume, we use the external cross section area at maximal shortening, because this is the maximum cross section area which the actuator should be allowed to occupy in a limb segment. For the nylon shell actuator, the cross section area is 0.95 cm^2 at 0.75 L_0, which yields the stiffness intensity of 331 N/L_0 cm^2, the maximum tension intensity of 116 N/cm^2, and the work per cycle per unit volume of 0.20 J/cm^3.

The above properties of the other two actuators (fiberglass shell and Bridgestone) are listed in Table I. The way that the threads form the external braided shell of the actuators influences most differences between the three actuators. The nylon shell actuator consists of the lowest thread density, lower thickness threads shell, which yields the widest 35% moving range, highest work density, and smallest Coulomb friction.

For biological muscles, the tension-length relation can be described by the "active tension" with a trapezoidal shape and the "passive tension" with increasing stiffness when stretched beyond a certain length. There may be a local maximum of the total tension if the increase of passive tension is less than the decrease of active tension to the length. The zero-tension lengths of the active tension are 0.64 and 1.8 L_0 (frog striated muscle, [5]), however, if we define the dynamic range of biological muscles by the nonnegative-slope region of the active tension-length curve, then it is within 0.64 to 1.12 L_0. The maximum tension intensity is about 35 N/cm^2 ([8], or 30 N/cm^2 from [6]), this yields the average stiffness intensity of 73 N/L_0 cm^2, and the work per cycle per unit volume of 0.13 J/cm^3 by numerically integrating the tension-length curve within the dynamic range.

In summary, the biological muscle can be stretched beyond its resting length much longer than the actuators. Also, the biological muscle can shorten a little more than the actuators This is a major disadvantage of the actuators. On the other hand, the tension intensity of the actuators is much higher than biological muscles, this is a major advantage of the actuators and yields higher work density and stiffness intensity. Finally, to improve the match to biological muscle static properties, passive parallel and serial elastic elements, which exist in biological muscles, can be added into the actuators without difficulty.

B. Dynamic Properties: Tension-Velocity Relationships, Power, and Response Time

The tension-velocity relation of the nylon shell actuator, if we do not count the viscosity of the pneumatic circuit, is dominated by a velocity-insensitive Coulomb friction, and the velocity-dependent viscous friction is immeasurable, which yields a very high maximum velocity in theory. The measured highest peak velocity is 6.19 L_0/s. The measured power per unit volume is 1.1 W/cm^3 in average of half cycle and 2.65 W/cm^3 in peak. For the full activation step response, the total delay time in above experiments is 12 ms, the tension rising time is 30 ms, and the falling time is 53 ms.

On the other hand, the hyperbolic tension-velocity curve of biological muscles indicates the viscosity decreases when the velocity increases [11], and there is no Coulomb friction reported. The typical maximum shortening velocity is 2 L_0/s for slow muscle and 8 L_0/s for fast muscle [18] or 20 L_0/s for fast muscle [6]. According to Hill's tension-velocity curve, the maximum peak power is about 0.1 $F_{\max} v_{\max}$ [14]. Applying

TABLE I
THE MECHANICAL PROPERTIES OF THE MCKIBBEN ACTUATORS AND BIOLOGICAL MUSCLES

properties	units	McKibben actuators @ 5 bar			Biological muscles
		Nylon shell	Fiberglass shell	Bridgestone	
Resting length (L_o)	cm	14.0	20.0	14.7	
Dynamic range	L_o	0.75 - 1.1	0.86-1.14	0.79 - 1.02	0.64 - 1.12
Maximum tension	N	110 @ 1.1 L_o	56 @ 1.15 L_o	260 @ 1.02 L_o	
Stiffness	N/L_o	314	200	1130	
Work per cycle	NL_o	19	7.8	30	
Cross section area	cm^2	0.95 @ 0.75 L_o	0.64 @ 0.85 L_o	2.0 @ 0.78 L_o	
Tension intensity	N/cm^2	116	88	130	35
Stiffness intensity	N/$L_o$cm^2	331	313	565	73
Work density per cycle	J/cm^3	0.20	0.12	0.15	0.13
Coulomb friction	N	2.5	5	5	0
Maximum velocity	L_o/s	> 6.19			2 - 8 or 20
Average power density	W/cm^3	1.1			
Peak power density	W/cm^3	2.65			0.70
Energy efficiency	-	0.32 - 0.49			0.2 - 0.25

35 N/cm^2 maximum tension intensity and 20 L_0/s maximum shortening velocity yields maximum peak power per unit volume of 0.70 W/cm^3 for skeletal muscle.

Obviously the tension-velocity relationship of the actuator is not similar to that of biological muscles. Fortunately, the viscous friction is much smaller and thus we can add some parallel viscous elements to simulate biological muscles. In addition, there may be some kinds of lubricant which can effectively reduce the Coulomb friction. Finally, The response time of biological muscles, although are not given here, have very wide range, and can be shorter in fast muscles than in the actuator.

C. Energy Efficiencies

The theoretical maximum energy efficiency of the nylon shell actuator is about 0.32 to 0.49. This seems higher than 0.2 to 0.25 of human muscles [8], [10]. However, the actual energy efficiency of the actuator will be lower due to additional nonideal energy losses.

D. Supplementary Pneumatic Elements

Besides the above considerations, the properties of the supplementary pneumatic elements must be considered, as well. The necessary elements include an electrovalve, tubing, and a high-pressure gas source.

The Festo MPP-3-1/8 electrovalve used in above experiments is 0.8 kg in weight, $14.5 \times 4.5 \times 4.5$ cm^3 in size, and it takes 0.95 A current at 18 V to get 600 l/min flow rate at 6.9 bar input without load. Another valve we tested (Animate Systems SARCOS servovalves C100P/80) is 0.1 kg in weight, $8.3 \times 1.9 \times 1.9$ cm^3 in size, takes 0.4 A at 5.8 V to get 23 l/min at the same conditions. The flow rate of the former is much higher with the costs of higher control energy and bigger size. Although the volume change of the actuator is small, or even zero, we should notice that gas is highly compressible, and the mass changes greatly when its pressure changes. The higher flow rate valve will shorten the system response time, and thus gives a closed loop controller more flexibility to remain stable. However, it is much heavier and bigger than the actuator. This will increase the total weight and size of the system, and also force the designer to avoid to put the valves on moving parts, thus long tubing must be used to connect each valve with each independent-controlled actuator. Also, the high control energy will reduce the energy efficiency of the whole system.

About the tubing, there may be many pieces of tubing, long and wrapping around, in a whole system. The gas viscosity inside tubing decreases while its diameter increases; however, its flexibility decreases at the same time. So, trade-off exists between high flexibility, in order not to disturb movement, and low viscosity, in order not to slow down response.

In order to drive several actuators for many shortening-lengthening cycles, there must be a gas reservoir with very high pressure and acceptable volume if there is no additional energy source. This will waste a lot of energy to compress gas above necessary operating pressure while preparing the high pressure source and yields a very poor energy efficiency. On the other hand, a compressor with motor or engine may

solve the poor energy efficiency problem; however, it may be heavy and noisy. Finally, a low-pressure reservoir with heating chamber may obtain the highest efficiency since the heat is converted directly to actuator's mechanical energy; however, the gas may be so hot to damage the actuator and injure the user.

VII. Conclusion and Future Work

The linearized mechanical model of the actuator and the lumped parameter model of the pneumatic system gave us simple yet accurate descriptions of the actuator and the pneumatic behaviors. Although no mechanical-pneumatic integrated model was shown, a model can be made by substituting the actuator for the accumulator, cascading the output of the pneumatic circuit model to the input of the actuator dynamic model, and adding a feedback pathway from the length of actuator to its volume (gas capacitance). This may be analogous to the mechanical coupling of calcium ion concentration (or active state) in real muscle [7], [19]. These models can be used in simulation of single or multiple actuator systems.

The static mechanical features of the actuator are very similar to biological muscles, except the dynamic range is narrower and the tension intensity is much higher. Some parallel and serial elastic elements may be added to fine tune the passive elastic characteristics. On the other hand, some dynamic features may need to be modified to get even closer. For examples: use lubricant to reduce the Coulomb friction and add some viscous material to increase the viscous friction in order to fit the tension-velocity relationship.

However, the pneumatic system, which provides control and power to the actuator, still needs a lot of improvement. For example: we need to find a lighter valve with acceptable flow rate, integrating the tubing into the muscle-bone assembly components to solve tubing length and wrapping problems, and find a light and quiet gas source with reasonable energy efficiency. Besides the actuator performance, these are also important factors which must be improved in order to implement a feasible muscle replacement system.

References

[1] R. E. Burke, P. Rudomin, and F. E. Zajac, "The effect of activation history on tension production by individual muscle units," *Brain Res.*, vol. 109, pp. 515–529, 1976.

[2] C.-P. Chou and B. Hannaford, "Dual stable point model of muscle activation and deactivation," *Biol. Cybern.* vol. 66, pp. 511–523, 1992.

[3] H. S. Gasser and A. V. Hill, "The dynamics of muscular contraction," in *Proc. R. Soc.*, 1924, vol. B96, pp. 398–437.

[4] M. M. Gavrilovic and M. R. Maric, "Positional servo-mechanism activated by artificial muscles," *Med. & Biol. Eng.*, vol. 7, pp. 77–82, 1969.

[5] A. M. Gordon, A. F. Huxley, and F. J. Julian, "The variation in isometric tension with sarcomere length in vertebrate muscle fibers," *J. Physiol.*, vol. 184, pp. 170–192, 1966.

[6] A. M. Gordon, "Contraction in skeletal muscle," in *Textbook of Physiology, Vol 1: Excitable Cells and Neurophysiology*, 21st ed. Philadelphia, PA: W. B. Saunders, 1989, ch. 8.

[7] A. M. Gordon and E. B. Ridgway, "Stretch of active muscle during the declining phase of the calcium transient produces biphasic changes in calcium binding to the activating sites," *J. Gen. Physiol.*, vol. 96, pp. 1013–1035, 1990.

[8] A. C. Guyton, "Contraction of skeletal muscle," in *Textbook of Medical Physiology*, 7th ed. Philadelphia, PA: W. B. Saunders, 1986, ch. 11.

[9] B. Hannaford and J. M. Winters, "Actuator properties and movement control: Biological and technological models" in *Multiple Muscle Systems*, J. Winters and S. Woo, Eds. New York: Springer-Verlag, 1990.

[10] A. V. Hill, "The maximum work and mechanical efficiency of human muscles and their most economical speed," *J. Physiol.*, vol. 56, pp. 19–41, 1922.

[11] ——, "The heat of shortening and the dynamic constants of muscle," in *Proc. R. Soc.*, 1938, vol. B126, pp. 136–95.

[12] K. Inoue, "Rubbertuators and applications for robots," in *Robotics Research: The 4th International Symposium*, R. Bolles and B. Roth, Eds. Cambridge, MA: MIT Press, 1988.

[13] A. Levin and J. Wyman, "The viscous elastic properties of muscle," in *Proc. R. Soc.*, 1927, vol. B101, pp. 218–243.

[14] T. A. McMahon, "Fundamental muscle mechanics," in *Muscle, Reflexes, and Locomotion*. Princeton, NJ: Princeton Univ. Press, 1984, ch. 1.

[15] J. Menkes, A. B. Cambel, and L. Talbot, "Gas dynamics," in *Fluid Mechanics Source Book*, S. P. Parker, Ed. New York: McGraw-Hill, 1988.

[16] L. F. Moody and N. J. Princeton, "Friction factors for pipe flow," *Trans. ASME*, vol. 66, p. 672, 1944.

[17] H. F. Schulte, Jr., "The characteristics of the McKibben artificial muscle," in *The Application of External Power in Prosthetics and Orthotics*. Washington, DC: Nat. Acad. Sci.-Nat. Res. Council, 1961.

[18] J. M. Winters, "Hill-based muscle models: A system engineering perspective," in *Multiple Muscle Systems*, J. Winters and S. Woo, Eds. New York: Springer-Verlag, 1990.

[19] G. I. Zahalak, "Modeling muscle mechanics (and energetics)," in *Multiple Muscle Systems*, J. Winters and S. Woo, Eds. New York: Springer-Verlag, 1990.

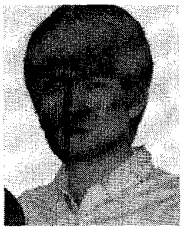

Ching-Ping Chou received the B.S. degree in electrical engineering from National Taiwan University, Taipei, R.O.C., in 1988, and the M.S. degree in electrical engineering from the University of Washington, Seattle, in 1991. He is now a Ph.D. candidate in the Department of Electrical Engineering, University of Washington.

His current research interests include pneumatic artificial muscles, human spinal cord neural circuitry and motion control, and physiologically analogous artificial neural network controller.

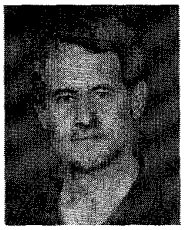

Blake Hannaford (S'82–M'85) received the B.S. degree in engineering and applied science from Yale University, New Haven, CT, in 1977, and the M.S. and Ph.D. degrees in electrical engineering from the University of California, Berkeley, in 1982 and 1985, respectively. At Berkeley he pursued thesis research in multiple target tracking in medical images and the control of time-out voluntary human movement.

Before graduate study, he held industrial positions in digital hardware and software design, technology analysis, and medical image processing. From 1986 to 1989 he worked on the remote control of robot manipulators in the Man-Machine Systems Group in the Automated Systems Section of the NASA Jet Propulsion Laboratory, California Institute of Technology, Pasadena. He supervised that group from 1988 to 1989. Since September 1989, he has been with the University of Washington, Seattle, where he has been Associate Professor of Electrical Engineering since 1993. His currently active interests include small scale telerobotics, biologically based design of robot manipulators, and force feedback for virtual environments.

Dr. Hannaford was awarded the National Science Foundation's Presidential Young Investigator Award and the Early Career Achievement Award from the IEEE Engineering in Medicine and Biology Society.